N89-20947

INVERSE WING DESIGN IN TRANSONIC FLOW INCLUDING VISCOUS INTERACTION*

Leland A. Carlson, Robert R. Ratcliff, and Thomas A. Gally
Texas A&M University
College Station, Texas

and

Richard L. Campbell
NASA Langley Research Center
Hampton, Virginia

SUMMARY

Several inverse methods have been compared and initial results indicate that differences in results are primarily due to coordinate systems and fuselage representations and not to design procedures. Further, results from a direct-inverse method that includes three-dimensional wing boundary-layer effects, wake curvature, and wake displacement are presented. These results show that boundary-layer displacements must be included in the design process for accurate results.

INTRODUCTION

Over the past several years, a variety of transonic wing design methods and computer codes (refs. 1-5) have been developed. In general, these methods solve the full potential flow equation and utilize the inverse approach in that pressure distributions are specified over all or part of the wing surface. Several include some of the effects of viscous interaction via strip boundary-layer calculations (ref. 1) or two-dimensional computations that include a correction for three-dimensional viscous effects (ref. 3). However, none of these methods includes a true three-dimensional boundary-layer calculation or the effects due to wake curvature, etc., which might have important effects on computed wing designs. In addition, they differ in the number and spacing of grid points, the design approach, the treatment of fuselage effects, and the control of trailing-edge thickness. Obviously whether or not these formulation differences significantly affect design results is of interest.

Currently, the design version of TAWFIVE (refs. 6-7), termed TAW5D (ref. 4), is being extended to include three-dimensional boundary-layer and wake viscous interaction effects and is being used to study various leading-edge relofting/trailing-edge control design procedures. As part of this study, it was believed that it would be interesting to investigate the consequences of differences in both numerical and physical formulations on the design process and resultant wing designs. Thus, this paper will present initial results of two ongoing studies. The first part will compare several inverse

*This work was supported by NASA Grant NSG 1-619.

design methods and their results, while the second portion will discuss the influence of viscous interaction on transonic wing design.

INVERSE METHOD COMPARISON STUDIES

The RAE Wing Body 'A' configuration (ref. 8) at a freestream Mach number of 0.8 and angle of attack of 2 degrees was selected as the test case for the comparison studies. The wing for this configuration has an aspect ratio of 5.5, a leading-edge sweep of 36.7 degrees, and a taper ratio of 0.375, is untwisted, and is composed of RAE 101 symmetrical airfoil sections. Three different inverse design methods were selected for the comparison, the direct-inverse curvilinear coordinate system TAW5D code (ref. 4), the stretched Cartesian grid direct-inverse ZEBRA method (ref. 2-3), and the inverse predictor-corrector FLO30DC approach (ref. 5); and their characteristics and features are listed on Table I.

In order to avoid the complexities associated with various viscous interaction schemes, it was decided to limit this comparison study to inviscid flow; and, since it was believed that one of the primary usages of design codes would be to modify only portions of wings, it was decided to design only between 30 and 70 percent span. The target pressure distribution for the design zone was obtained from an inviscid analysis by the TAW5D code (essentially TAWFIVE, ref. 7), which indicated that the flowfield at the selected conditions was slightly supercritical and that the wing lift coefficient was 0.210. In addition, the starting airfoil shapes were the correct 9% thick sections from root to 30% span, linearly thinning down to a 6% thick symmetrical section at 50% span and back to 9% at 70% span, followed by the correct sections on the outboard portions of the wing.

For the design studies, TAW5D was operated in the span lofting mode in which pressures were only specified at 30, 50, and 70% span. Under this procedure, airfoils were only inversely designed at these stations; and after each design update, in between sections were obtained by linear spanwise lofting. In all cases, the flow at these in between stations was computed in the direct-analysis mode. On the other hand, in the ZEBRA method, pressures were specified at each spanwise station from 30 thru 70%; and in the predictor-corrector, FLO30DC the pressure was specified and an airfoil section designed only at the 50% span location, with linear span lofting to 30% and 70% respectively. In all cases, leading-edge relofting options were selected in order to force the designs to have the proper trailing-edge thicknesses.

PROBLEMS

In setting up the test cases, several interesting problems were encountered. First, analysis computations of the RAE 'A' wing/body configuration by the ZEBRA and TAW5D codes yielded slightly different pressure distributions; and, in order to minimize these differences, the angle of attack used in ZEBRA was decreased to 1.8 degrees so as to match

the wing CL predicted by TAW5D. The corresponding pressure distributions are shown on figure 1; and since both methods solve the same equation, the variations must be due to differences in grid, fuselage, and boundary condition treatments. Near the root, ZEBRA predicts a greater fuselage effect in that the flow is more accelerated on the upper surface; while outboard, the leading-edge grid clustering inherent in TAW5D results in better resolution of the leading-edge region and minimum pressure peak. Near the trailing edge, where the ZEBRA coordinate system is actually finer, there are also some variations in the predicted pressures. However, between 30 and 70% span the two methods are in reasonable agreement, and meaningful design studies for this region should be possible.

The second problem was that FLO30DC could only handle for this case an infinite cylinder fuselage; and, thus, TAW5D and ZEBRA were "modified" to have as an option an infinite fuselage as well as a finite one. Figure 2 compares at the 50% span station on the RAE configuration the pressure distributions calculated by TAW5D associated with these two fuselages, and it can be seen that the effect is only a slight shift in the pressure coefficient level. This trend was true at all span stations, and overall wing and section lift coefficients were essentially identical. Nevertheless, as a result of these differences, two sets of target pressures for the design region were generated, one for the finite wing/body configuration and one for the infinite cylinder fuselage; and these were used as input into the appropriate versions of the codes.

RESULTS AND COMPARISONS

Figures 3-5 show results obtained at the design stations using the TAW5D method. In this case, each section was designed from 10% chord to the trailing edge and leading-edge relofting was utilized to force trailing-edge closure. However, the actual ordinate of the trailing edge was not specified. As can be seen, the starting profiles were a linear variation from the correct section at 30% and 70% span down to a thin symmetrical section at mid-span. While the 30 and 70% stations started with the correct shapes, they were design stations and could and did change during the computation. However, as shown on the figures, all three sections converged to the target shapes; and results for the finite fuselage and infinite fuselage cases were indistinguishable.

Results were also obtained with the ZEBRA code for both the infinite and finite body cases and by the FLO30DC code for the infinite cylinder fuselage using the appropriate pressure inputs. Figures 6-8 compare the designed sectional shapes obtained by the three codes for the infinite fuselage. It should be noted that the ZEBRA results were well converged having maximum ordinate changes of less than 1E-6 of chord when computations were terminated. Also, it can be seen that the FLO30DC and TAW5D results (denoted as CAMPBELL and TAWFIVE on the figures) are virtually identical, even though the methods used entirely different design procedures.

At the 30% span station, the lower surface profile predicted by ZEBRA is in agreement with the other methods, but on the upper surface it is considerably different. Examination of the pressure profiles on figure 1 indicate that at 30% TAW5D and ZEBRA analysis results agree on the lower surface but disagree on the upper. Consequently, when the TAW5D pressures are used as design input to ZEBRA, it is not surprising that a slightly different airfoil section resulted. At 50%, figure 7, where analysis results are in better agreement, particularly on the upper surface, the three methods predict virtually identical upper surfaces although the ZEBRA lower surface profile is slightly thicker; and at 70% span the ZEBRA prediction is again slightly thicker. (Similar differences between TAW5D and ZEBRA were obtained for the finite fuselage case.) Since TAW5D and ZEBRA use similar design procedures and TAW5D and FLO30DC have similar grids and body representations, it can be concluded that the differences in profile shapes portrayed in figures 6-8 are primarily due to coordinate system and fuselage representations.

In order to see infinite versus finite fuselage effects, the infinite cylinder fuselage wing pressures were used as input into both the infinite cylinder and wing/body versions of TAW5D; and a typical result is shown on figure 9. Here the infinite cylinder result is the "correct" profile; and as can be seen, the finite fuselage result is thinner and significantly different near the trailing edge. In fact, at the 30 and 70% stations, the upper and lower surfaces criss-crossed before coming together to satisfy trailing-edge closure. It is believed that this result demonstrates an important effect often encountered in inverse design, i.e., when a pressure distribution that is somehow incompatible with either physical reality or the computational model (in this case the fuselage representation) is used as input, the effect is almost always observed as either unrealistic profiles near the trailing edge or in the inability of the design process to satisfy the design input pressures near the trailing edge or both. In many cases, the "problem" can be solved by slight adjustments in the specified pressure distribution.

Now even though figures 6-8 show that the methods predicted different profiles, the significance of these differences can only be determined by an analysis of the designed wings and a comparison of the analysis results with the desired targets. Since TAW5D had previously been shown to be self consistent (ref. 4) and since the wing designed by TAW5D, fig. 3-5, had the correct airfoil sections, no analysis results for the TAW5D design are presented. However, figures 10-14 compare the target pressure distributions with analysis results by both TAW5D and ZEBRA for the wing designed by ZEBRA, which had different profile sections in the design region. First, it should be noted that in the design region, figures 11-13, the ZEBRA analysis agrees with the target pressure values for the inverse design zone, which extends from 0.1 chord to the trailing edge. This agreement indicates that the ZEBRA method did indeed satisfy the desired pressure boundary conditions. Second, due to inherent grid clustering near the leading edge, the TAW5D analysis of the ZEBRA design probably gives better resolution in the leading-edge region; and, finally, if it is assumed that the TAW5D analysis is the "most accurate" of the methods due to its fuselage and

boundary condition representations, then it is apparent from figures 10-14 that the ZEBRA design closely matches the target pressure distributions and lift coefficients. Overall, the TAW5D analysis of the ZEBRA design predicted a wing lift coefficient of 0.203 compared to the target value of 0.210; and similar results were obtained for both the finite and infinite fuselage cases. In many respects these good results are somewhat surprising considering the airfoil section differences on figures 6-8. In any event, the results shown on figures 10-14 are probably indicative of the level of agreement to be expected when using design methods differing in coordinate systems and fuselage treatment.

To conclude this section, it is believed that the results presented demonstrate the following:

(1) Inverse methods using similar coordinate systems and flow solvers will yield the same wing designs, and

(2) Inverse methods having different coordinate systems and fuselage representations but similar design procedures will yield different section profiles, but the pressure distributions and lift coefficients will be in reasonable agreement.

VISCOUS INTERACTION STUDIES

The configuration selected for these studies was the Lockheed Wing A wing-body (ref. 4 and 7) at a freestream Mach number of 0.8, an angle of attack of 2 degrees, and a mean chord Reynolds number of 24 million. The wing for this combination is composed of supercritical aft-cambered sections and has a quarter chord sweep of 25 deg., a linear twist distribution ranging from 2.28 deg. at the wing body junction to -2.04 deg. at the wing tip, an aspect ratio of eight, and a taper ratio of 0.4. Target pressure distributions were generated by an analysis using TAW5D with full boundary-layer and wake viscous interaction effects. As before, wing design was only between 30 and 70% span, target pressures were specified at 30,50 and 70%, and the span lofting technique described above was utilized. However, in order to properly include viscous interaction, after each boundary layer and wake update, displacement thicknesses were added to the airfoil ordinates at each analysis station to provide the correct displacement surface. Likewise, since at the design stations the displacement surface is the surface computed, the displacement thicknesses were subtracted to yield the ordinates of the actual airfoil at those locations. In addition, leading-edge relofting was utilized in order to obtain proper trailing-edge behavior. However, contrary to the situation for inviscid cases, convergence problems were observed when only the trailing-edge thicknesses were specified. Consequently, the actual trailing-edge ordinates desired at the design stations were specified.

STARTING PROFILE EFFECTS

Obviously, the initial airfoil section profiles should not affect the final designed sections; and, consequently, two cases were studied having significantly different starting profiles. The results for the first case

are shown on figures 15-17, and as can be seen the initial sections linearly varied from the correct aft-cambered profile at 20% span to a conventional non-aft cambered section at mid-span back to the correct aft-cambered section at 80% span. Here, the inverse design procedure started at 0.1 chord; and the initial leading edge at each design station was thinner than the target shape. As shown on the figures, the target sections and designed sections are in excellent agreement, particularly considering the extensive curve fits and interpolations involved in the design and viscous interaction procedures.

For the second test, the initial sections consisted of the correct profiles inboard from the root to 20% and outboard from 80% to the wing tip. However, as shown on figures 18-20, from 30% span through 70% span the initial sections were NACA 0012 airfoils; and linear lofting was used between 20 and 30% and 70 and 80%. In this case the inverse design procedure started at 0.04 chord, and the initial leading edge at each design station was thicker than the target section. As can be seen, the final designed sections are in excellent agreement with the target shapes, particularly in the leading-edge and cove regions.

It should be noted that in both of these cases, the section and wing lift coefficients and the section pressure distributions were essentially identical to the target values. Based upon these results, it is believed that the present viscous inverse design procedure can yield correct target profiles independent of initial airfoil section shapes.

BOUNDARY-LAYER AND WAKE EFFECTS

Studies conducted under the present program have indicated that design including full viscous interaction effects is more computationally intensive and that convergence is slower. Consequently, it was decided to compare the full viscous interaction design results with those obtained including viscous boundary-layer interaction but excluding wake effects and with those obtained assuming inviscid flow. For each case, the input pressure distributions were identical and corresponded to those predicted by a full viscous analysis of the Lockheed Wing A wing/body since those should be the closest to reality. The starting section profiles were those shown on figures 15-17, and the design region was from 30 to 70% span. As before, span relofting and leading-edge relofting were both used in all three cases.

The final section profiles resulting from these computations are shown on figures 21-23, and at all design stations the sections obtained by ignoring wake effects are very close but slightly thicker than those corresponding to the full viscous case. Further, while the inviscid case profile is very close to the others at 50% span, they are significantly different from those including viscous effects at 30 and 70% span. The results at 50% are not surprising since at that station the boundary layer is relatively thin over much of the surface and the design is strongly influenced by the viscous pressure boundary conditions at 30 and 70% span. However, the cove region is not well predicted; and, as can be seen on figure 22, the upper surface inviscid profile here is thinner than the full

viscous result, rather than thicker as would normally be expected. In this case, specification of the trailing-edge ordinate and use of relofting has forced a change in the leading-edge shape such that the final inviscid case airfoil upper surface is slightly thinner than expected.

At the 30 and 70% stations, it is believed that the shapes predicted by the inviscid computation are due to the fact that these design locations sense the viscous pressures specified at 50% but are strongly influenced by the inviscid pressures computed inboard and outboard respectively. In other words, as shown in the analysis case in reference 6, three-dimensional viscous effects also appear to be very important in the design case. Based upon these results, it appears that the effect of wake curvature and displacement on the airfoil section designs is relatively small. However, if the flowfield is assumed to be inviscid and only a portion of the wing is designed, the use of realistic pressure distributions as input to design stations may lead to unusual or even erroneous profiles, particularly at the boundaries of the design region.

ANALYSIS AND COMPARISON OF DESIGNS

As in the code comparison studies, the effect of including or excluding viscous effects can only be determined by comparing analysis results for the designed wings. Consequently, each of the wings portrayed on figures 21-23 was analyzed using TAW5D including boundary-layer interaction and wake displacement and curvature effects. Full viscous interaction effects were included because it was believed that such a representation would be the most realistic representation of the actual flow to be expected about the designed wing/body combination. The results of these analyses are shown in Table II and on figures 24-28. On these figures, the viscous pressures are very close to the target pressures; and comparison of the pressure distributions and sectional lift coefficients indicates that from a practical standpoint the differences between full viscous design and design including wing boundary layer but excluding wake effects is negligible.

However, analysis of the inviscidly designed wing indicates that in the design region, figures 25-27, the sections determined by inviscid design have lower than expected lifts and pressure distributions significantly different than the targets. (At this point, it should be noted that the "inviscid" curves on figures 24-28 are from a full viscous analysis of the inviscidly designed wing and are not the result of an inviscid analysis.) In addition, three-dimensional effects lead to lift losses and more forward shock locations on the sections inboard and outboard of the design region, even though these sections have the correct airfoil shapes. As can be seen, the effect is particularly significant on the outboard region. It should be noted that this decrease in lift due to designing inviscidly instead of including viscous effects is consistent with results previously obtained for airfoils (ref. 9).

It is believed that these initial results demonstrate the following:

(1) Section profiles for wings in transonic flow can be designed using the direct-inverse technique including the interaction effects of the three-dimensional wing boundary-layer and wake curvature and displacement. The resulting profiles are independent of the starting shapes.

(2) For the conditions considered, wake effects have very little effect on the designed airfoil shapes or on the wing pressure distributions.

(3) For the conditions considered, at least the wing boundary-layer displacement effect must be included in the design process. Otherwise, the designed wing will have less lift and different pressure distributions than desired.

CONCLUDING REMARKS

In summary, several inverse methods have been compared and initial results indicate that differences in results are primarily due to coordinate systems and fuselage representations and not to design procedures. Also, results from an inverse method that includes three dimensional wing boundary-layer effects, wake curvature, and wake displacement have been presented. These results show that boundary-layer displacements must be included in the design process for accurate results.

REFERENCES

1. Henne, P. A.: Inverse Transonic Wing Design Method. Journal of Aircraft, vol. 18, no. 2, February 1981, pp. 121-127.

2. Weed, R. A., Carlson, L. A., and Anderson, W. K.: A Direct-Inverse Three Dimensional Transonic Wing Design Method for Vector Computers. AIAA Paper No. 84-2156, August 1984.

3. Carlson, L. A. and Weed, R. A.: Direct-Inverse Transonic Wing Analysis-Design Method with Viscous Interaction. Journal of Aircraft, vol. 23, no. 9, September 1986, pp. 711-718.

4. Gally, T. A. and Carlson, L. A.: Inviscid Transonic Wing Design Using Inverse Methods in Curvilinear Coordinates. AIAA Paper No. 87-2551, August 1987.

5. Campbell, R. L. and Smith, L. A.: A Hybrid Algorithm for Transonic Airfoil and Wing Design. AIAA Paper No. 87-2552, August 1987.

6. Streett, C. L.: Viscous-Inviscid Interaction for Transonic Wing-Body Configurations Including Wake Effects. AIAA Journal, vol. 20, no. 7, July 1982, pp. 915-923.

7. Melson, N.D. and Streett, C. L.: TAWFIVE: A Users' Guide. NASA Technical Memorandum 84619, September 1983.

8. Treadgold, D. A., Jones, A. F., and Wilson, K. H.: Pressure Distribution Measured in the RAE 8'x6' Transonic Wind Tunnel on RAE Wing 'A' in Combination with an Axisymmetric Body at Mach Numbers of 0.4, 0.8, and 0.9. Experimental Data Base for Computer Program Assessment, Appendix B1, AGARD-AR-138, May 1979, pp. B4-1 -B4-25.

9. Carlson, L. A.: Inverse Transonic Airfoil Design Including Viscous Interaction. NASA CP-2001, Vol. 4, November 1976, pp. 1387-1395.

TABLE I. -- CHARACTERISTICS OF INVERSE METHODS

Method	TAW5D	ZEBRA	FLO30DC
Coordinate System	Body Fitted	Stretched Cartesian	Body Fitted
Boundary Conditions	On Surface	At Z = 0	On Surface
Fuselage	General Shape	Axisymmetric Body Approx. by Source/Sinks	Infinite Cylinder
Design Method	Direct-Inverse	Direct-Inverse	Predictor-Corrector
Grid	160x24x32	90x30x30	160x24x32
Points on Airfoil Section	105 with LE Clustering	100 almost equally spaced	105 with LE Clustering
Number of Span Stations	21	21	21

TABLE II. -- RESULTS OF ANALYSIS OF DESIGNED WINGS

	Target	Full Viscous Design	No Wake Design	Inviscid Design
cl at 50%	.514	.509	.506	.427
Wing CL	.483	.478	.477	.419

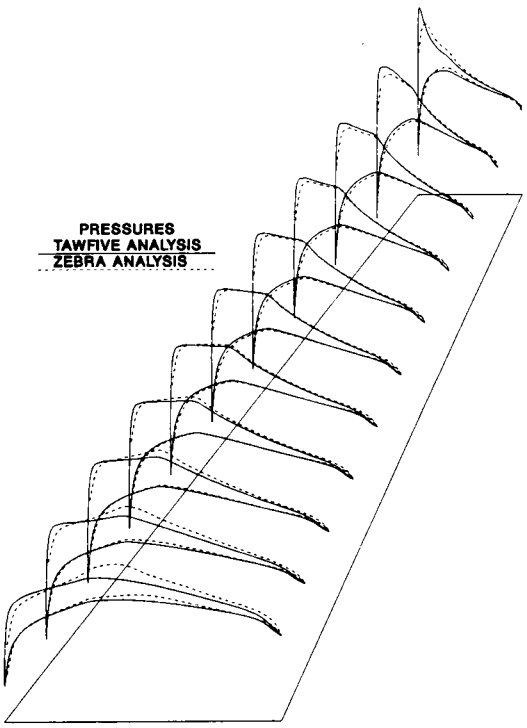

Figure 1. Comparison of analysis results for RAE wing body 'A' at Mach No. = 0.8, AOA = 2 degrees.

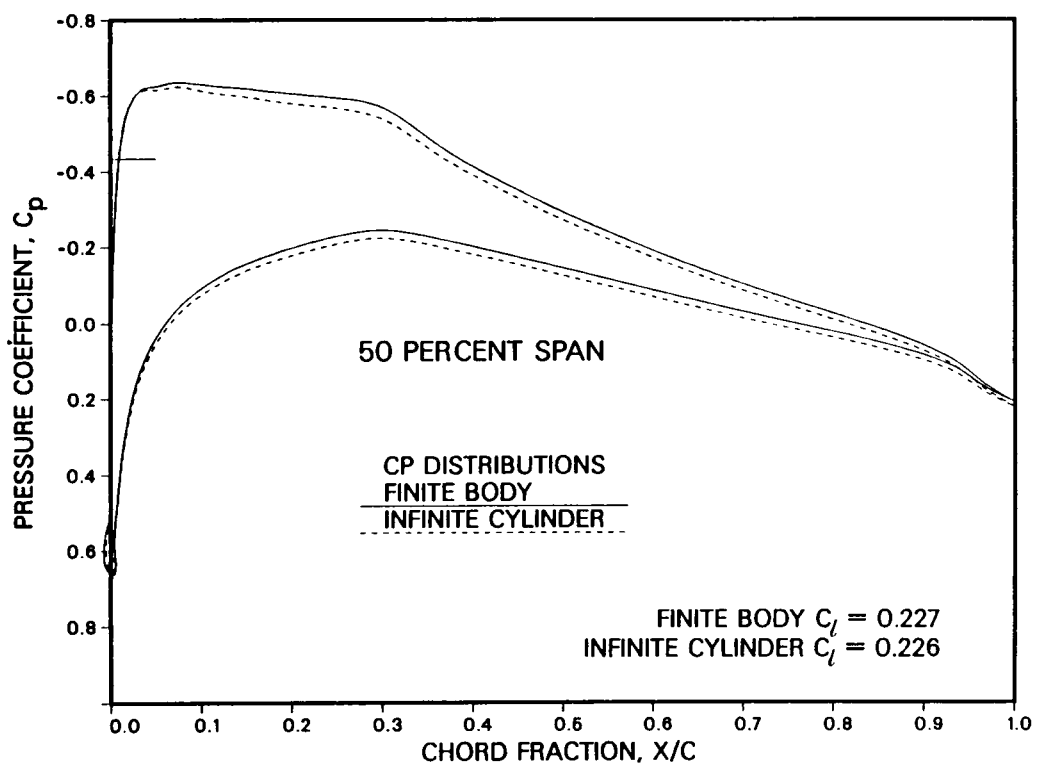

Figure 2. Comparison of finite fuselage midspan pressures with infinite cylinder fuselage results for RAE wing body 'A'.

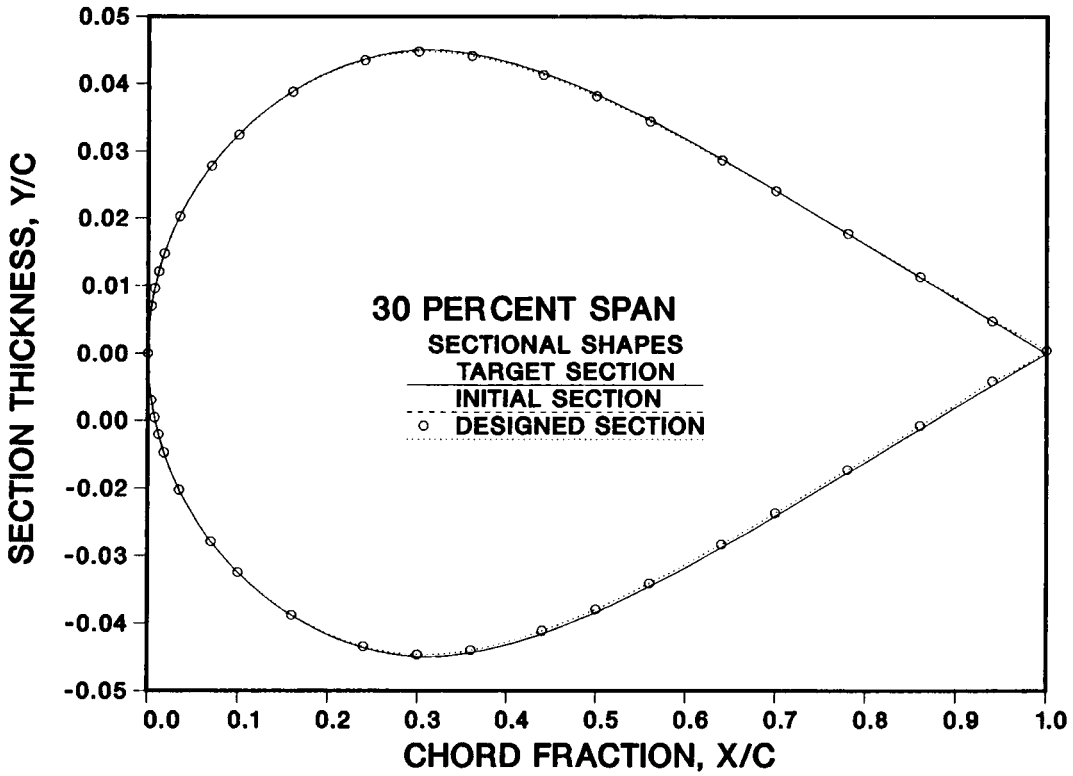

Figure 3. Comparison of section designed by TAW5D at 30 percent span for RAE wing body 'A' with initial and target sections.

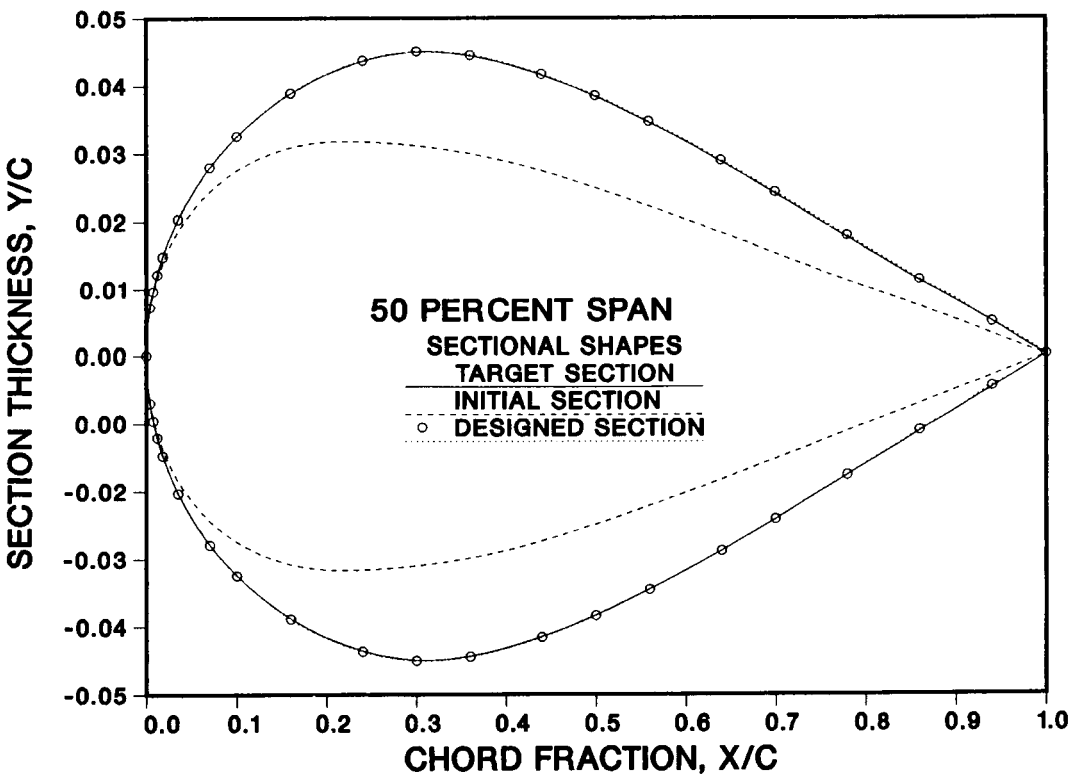

Figure 4. Comparison of section designed by TAW5D at 50 percent span for RAE wing body 'A' with initial and target sections.

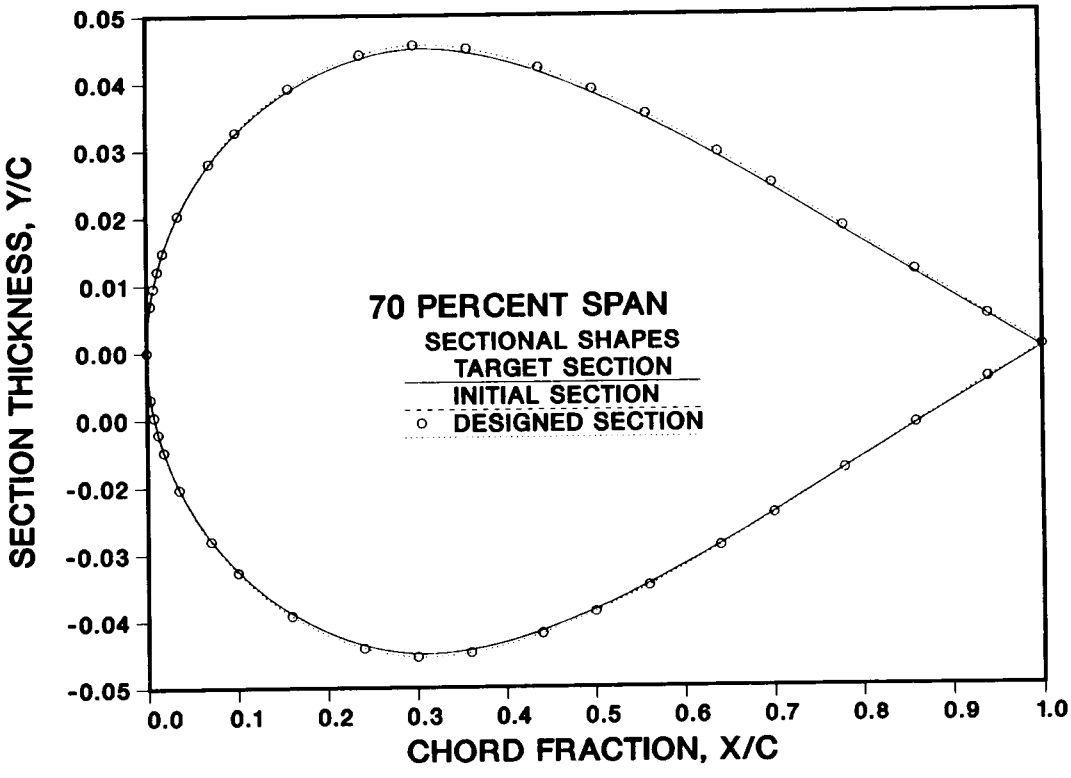

Figure 5. Comparison of section designed by TAW5D at 70 percent span for RAE wing body 'A' with initial and target sections.

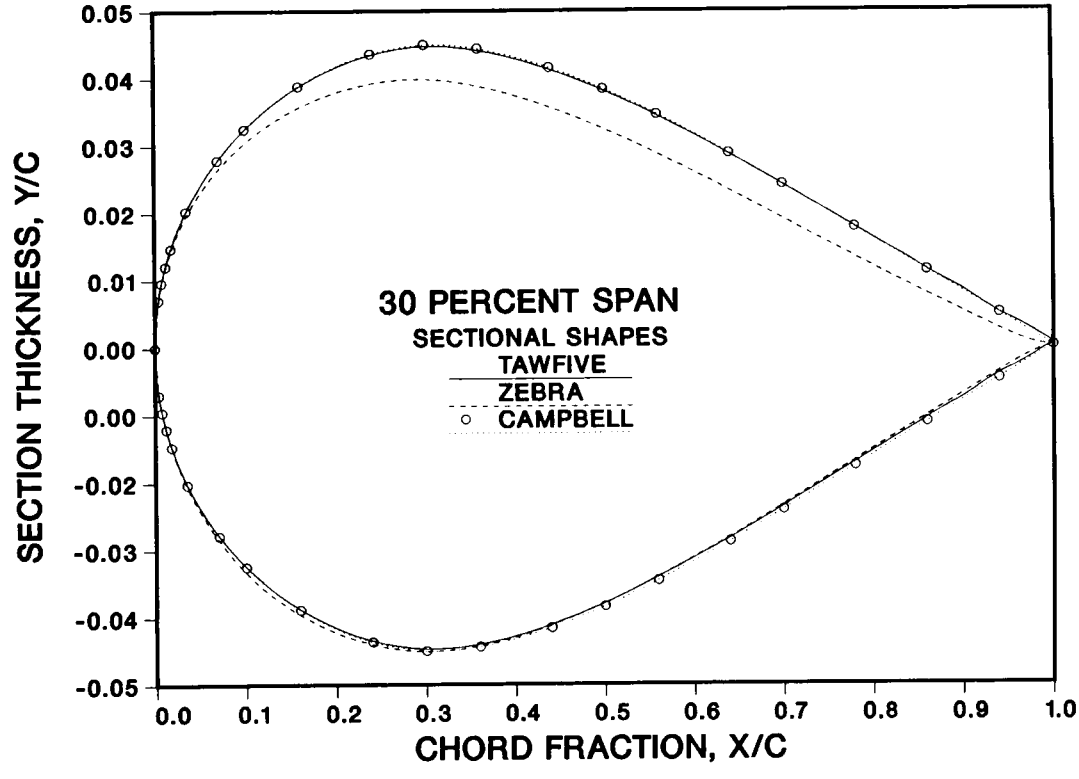

Figure 6. Comparison of sections designed by different methods at 30 percent span for RAE wing 'A' with infinite fuselage.

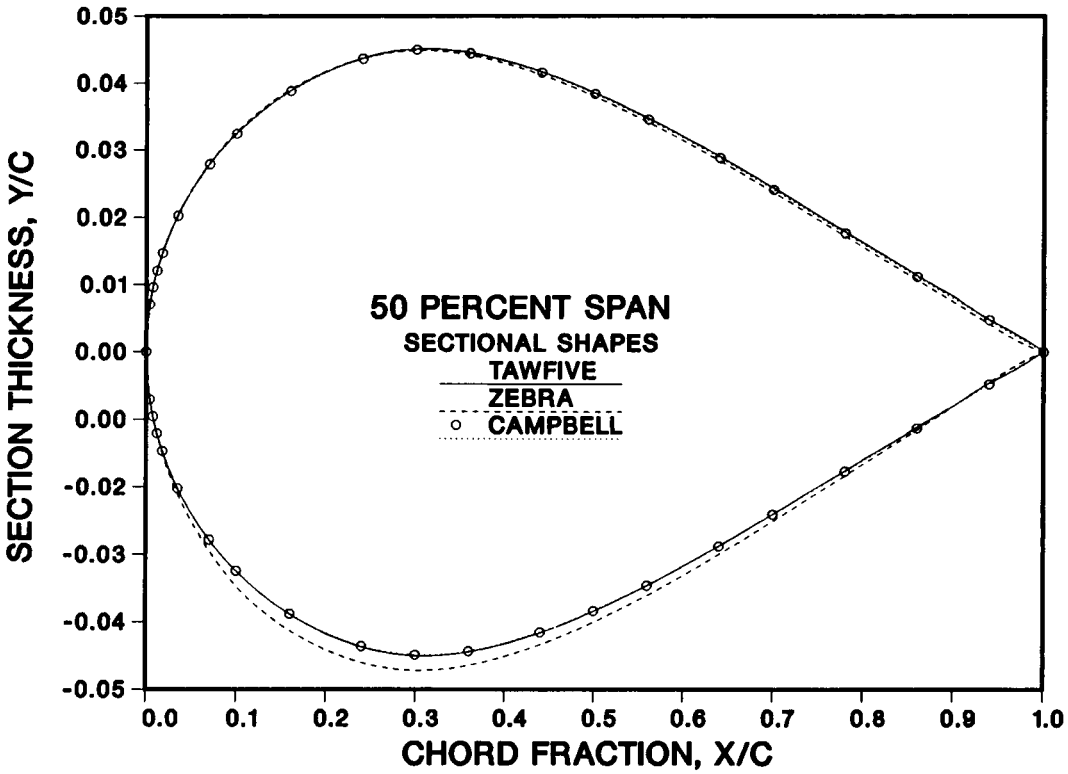

Figure 7. Comparison of sections designed by different methods at 50 percent span for RAE wing 'A' with infinite fuselage.

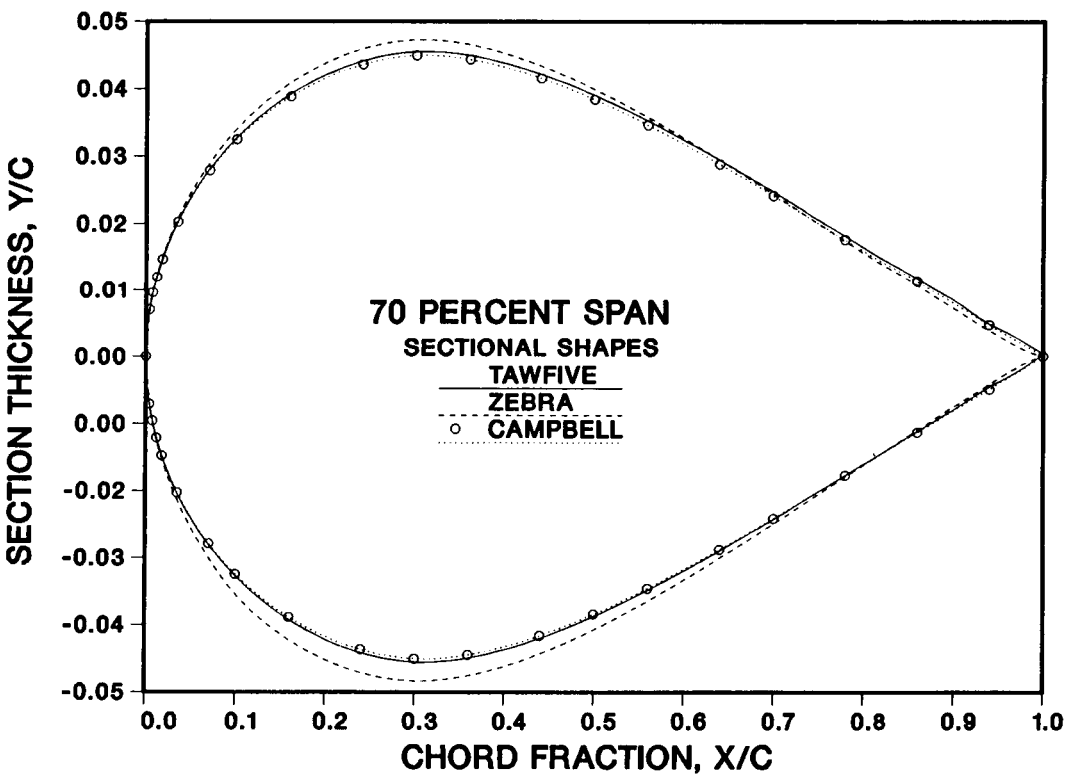

Figure 8. Comparison of sections designed by different methods at 70 percent span for RAE wing 'A' with infinite fuselage.

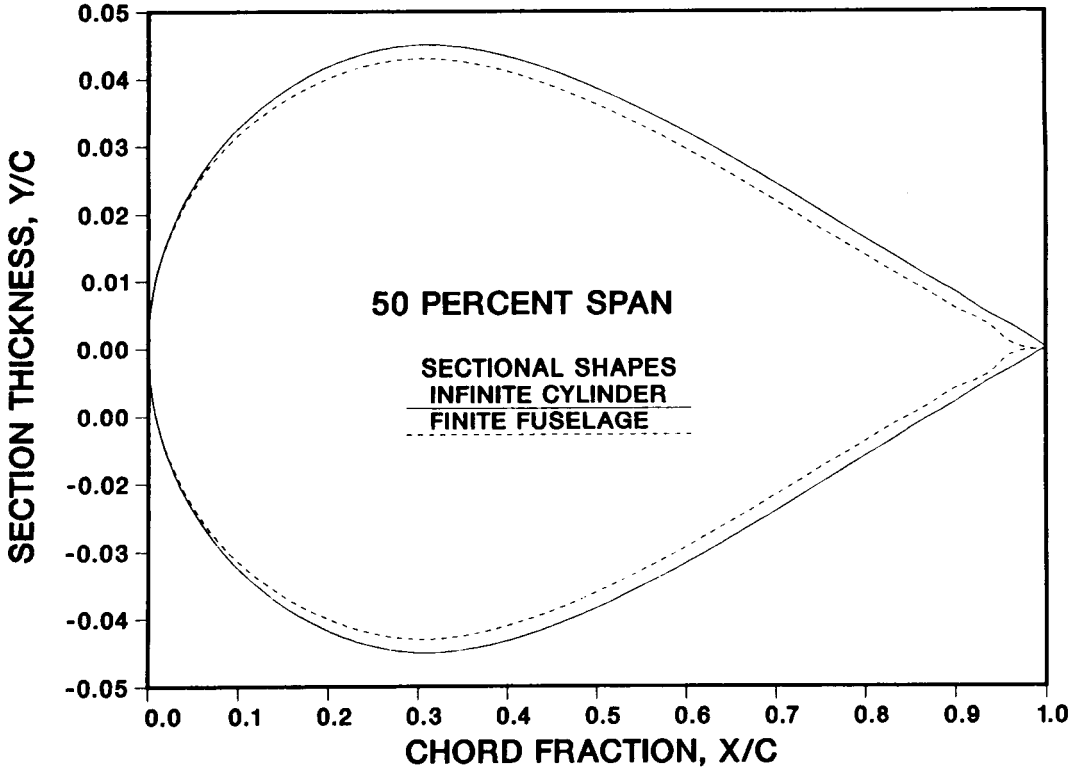

Figure 9. Comparison of sections designed by finite and infinite fuselage versions of TAW5D using infinite fuselage wing pressures as input in both cases (RAE wing 'A').

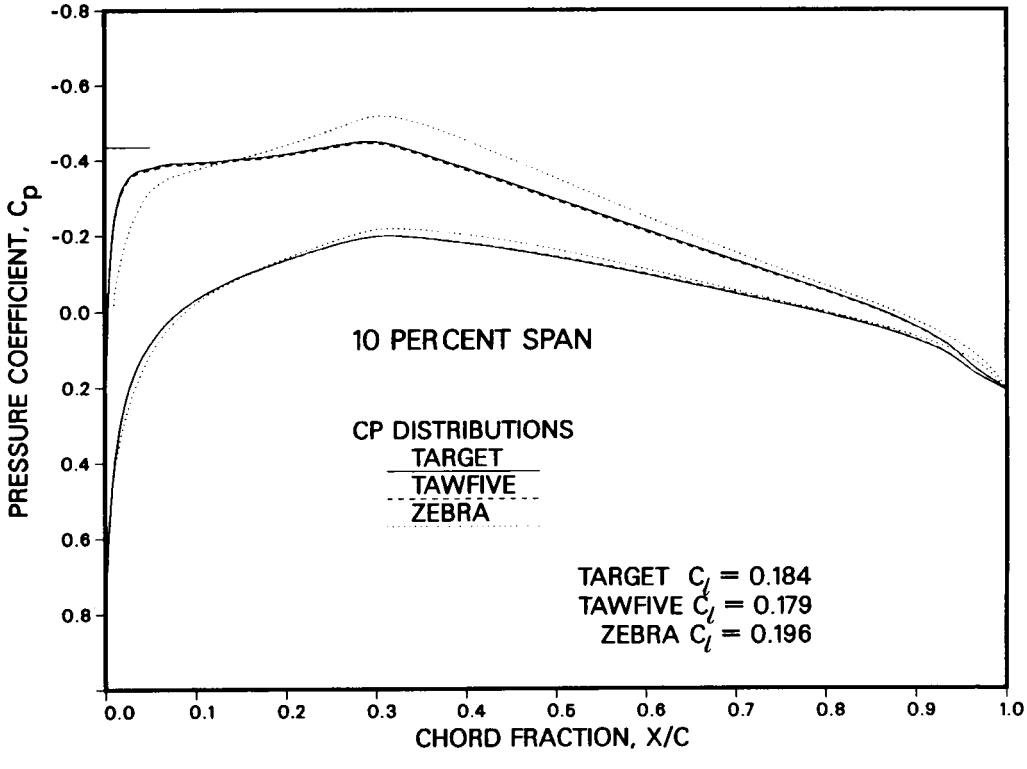

Figure 10. Comparison at 10 percent span of target values with pressures obtained by analyses of the wing designed by ZEBRA (RAE wing body 'A', Mach = 0.8, AOA = 2 degrees).

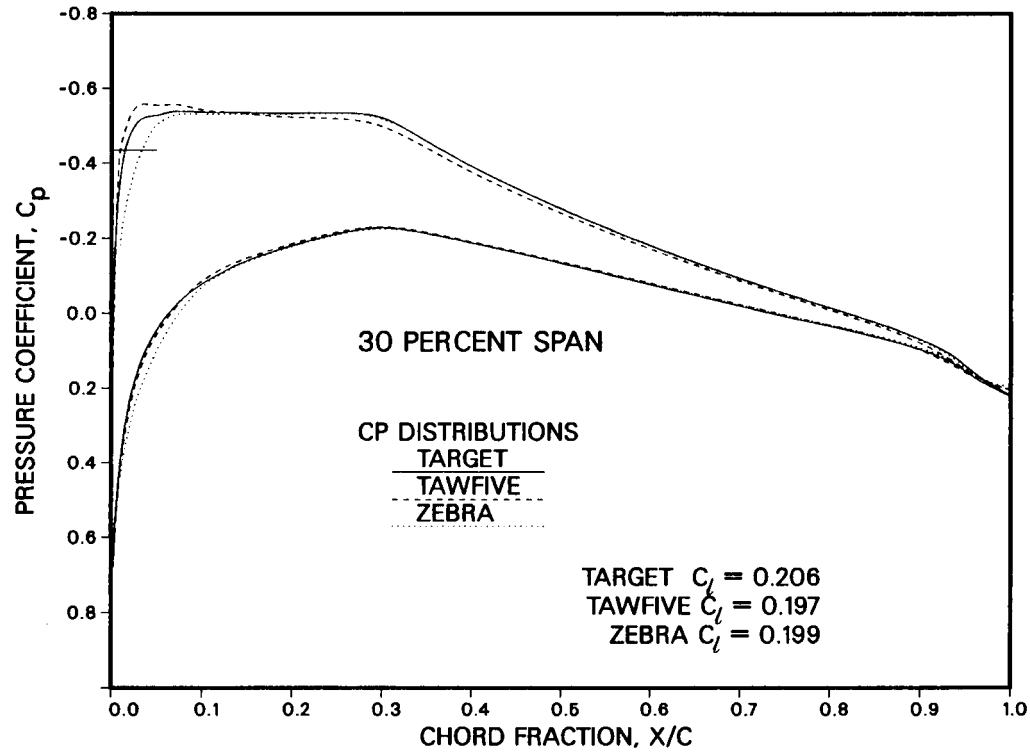

Figure 11. Comparison at 30 percent span of target values with pressures obtained by analyses of the wing designed by ZEBRA (RAE wing body 'A', Mach = 0.8, AOA = 2 degrees).

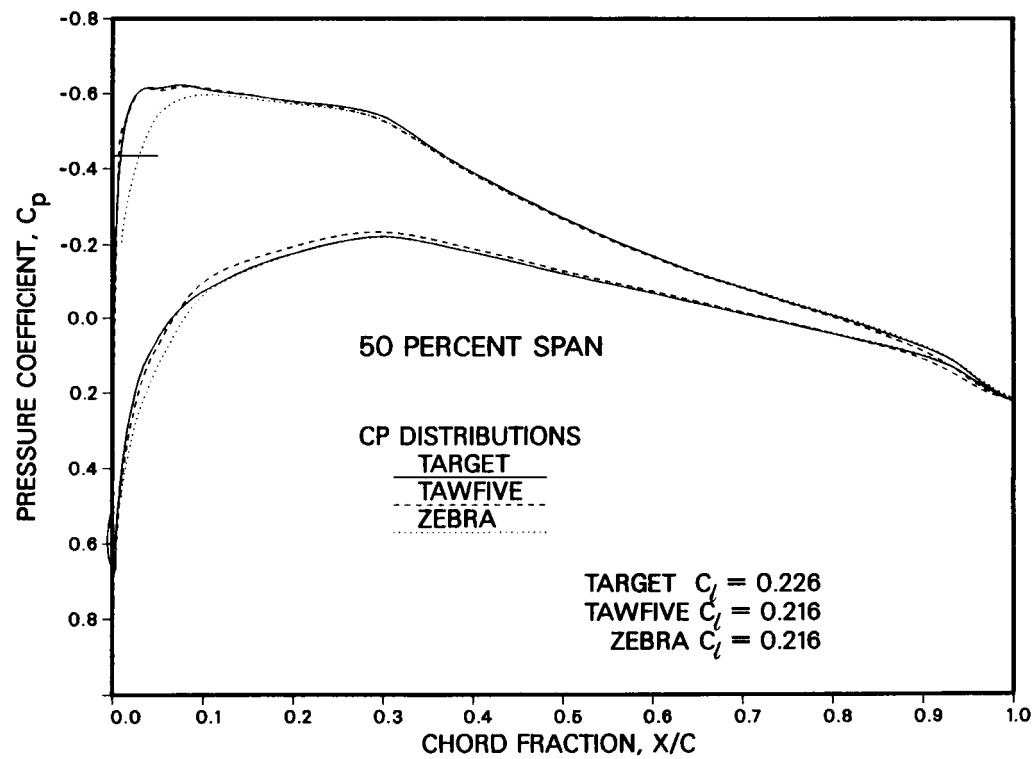

Figure 12. Comparison at 50 percent span of target values with pressures obtained by analyses of the wing designed by ZEBRA (RAE wing body 'A', Mach = 0.8, AOA = 2 degrees).

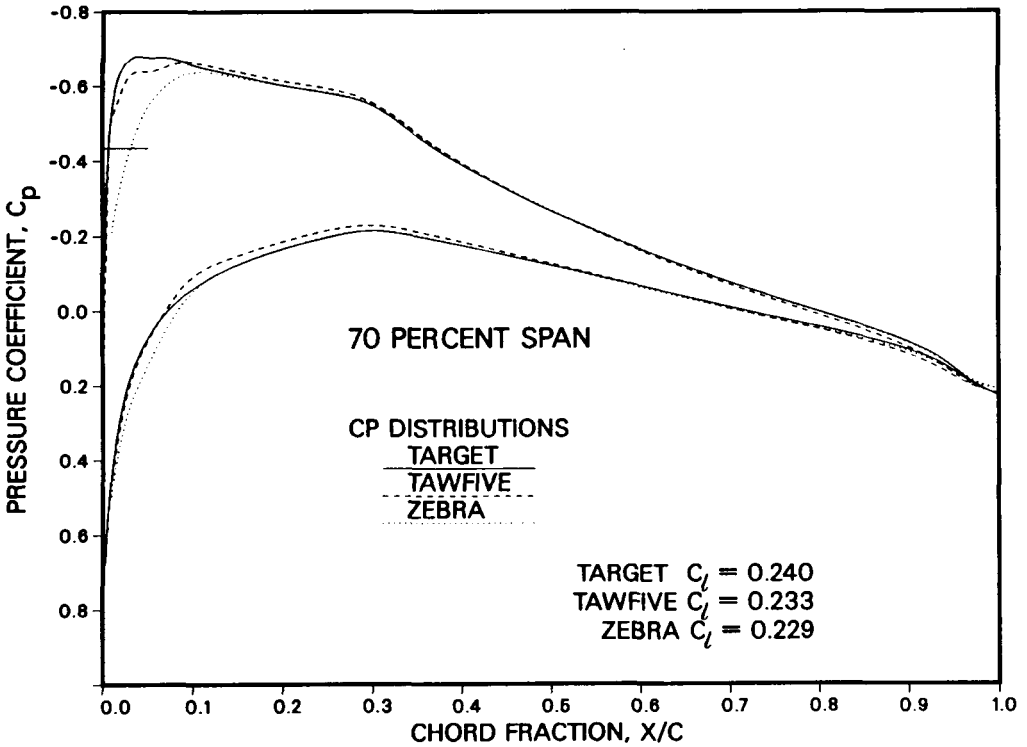

Figure 13. Comparison at 70 percent span of target values with pressures obtained by analyses of the wing designed by ZEBRA (RAE wing body 'A', Mach = 0.8, AOA = 2 degrees).

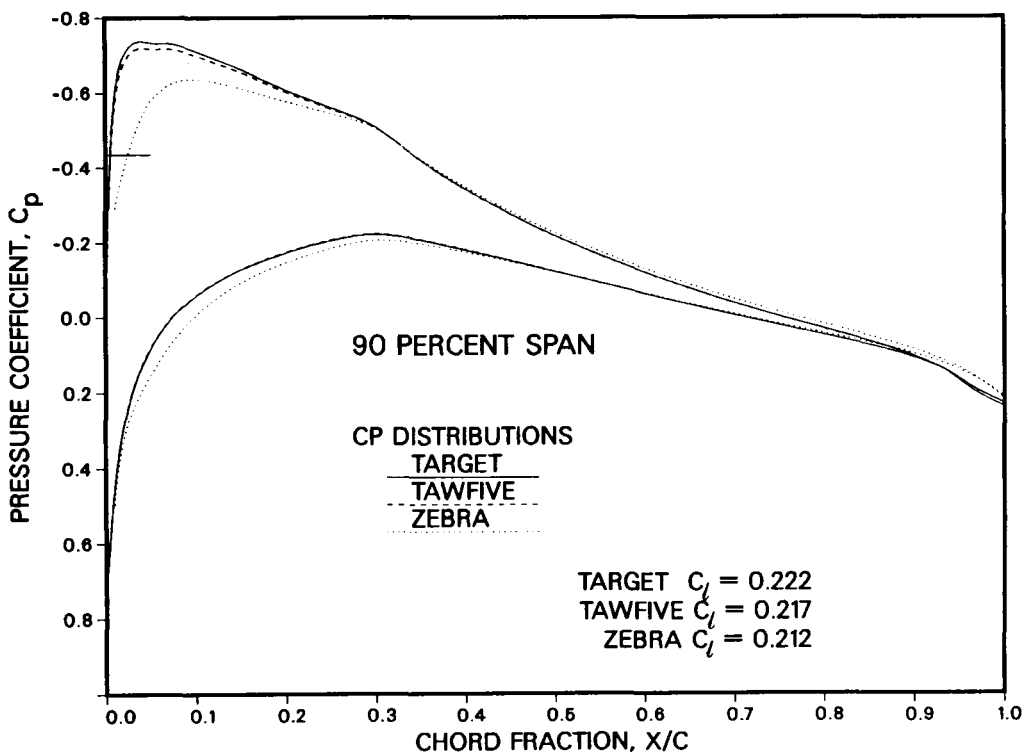

Figure 14. Comparison at 90 percent span of target values with pressures obtained by analyses of the wing designed by ZEBRA (RAE wing body 'A', Mach = 0.8, AOA = 2 degrees).

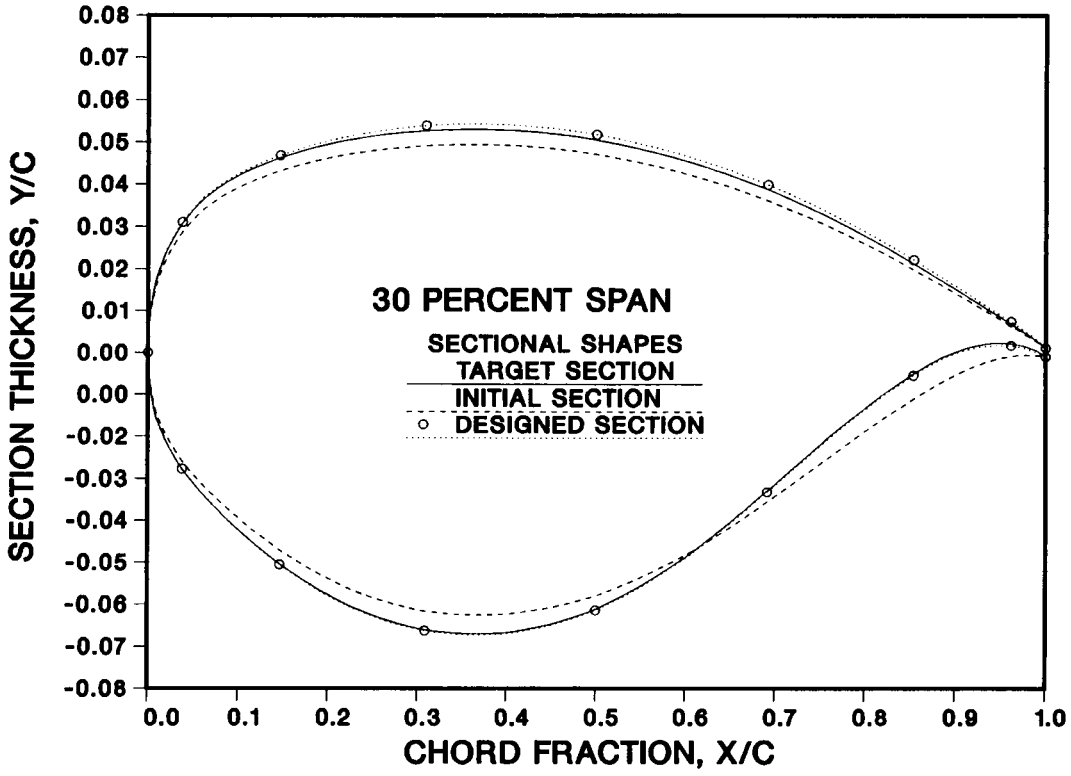

Figure 15. Comparison of section designed by TAW5D at 30 percent span for Lockheed Wing A wing body with target and first type of initial section.

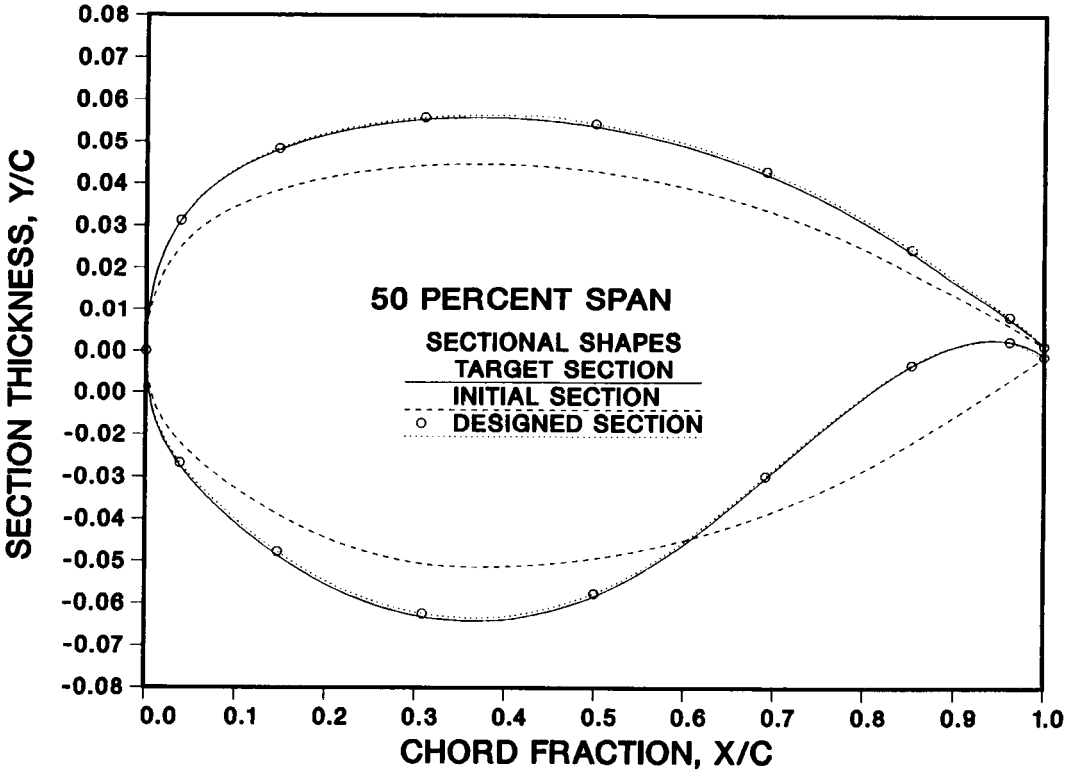

Figure 16. Comparison of section designed by TAW5D at 50 percent span for Lockheed Wing A wing body with target and first type of initial section.

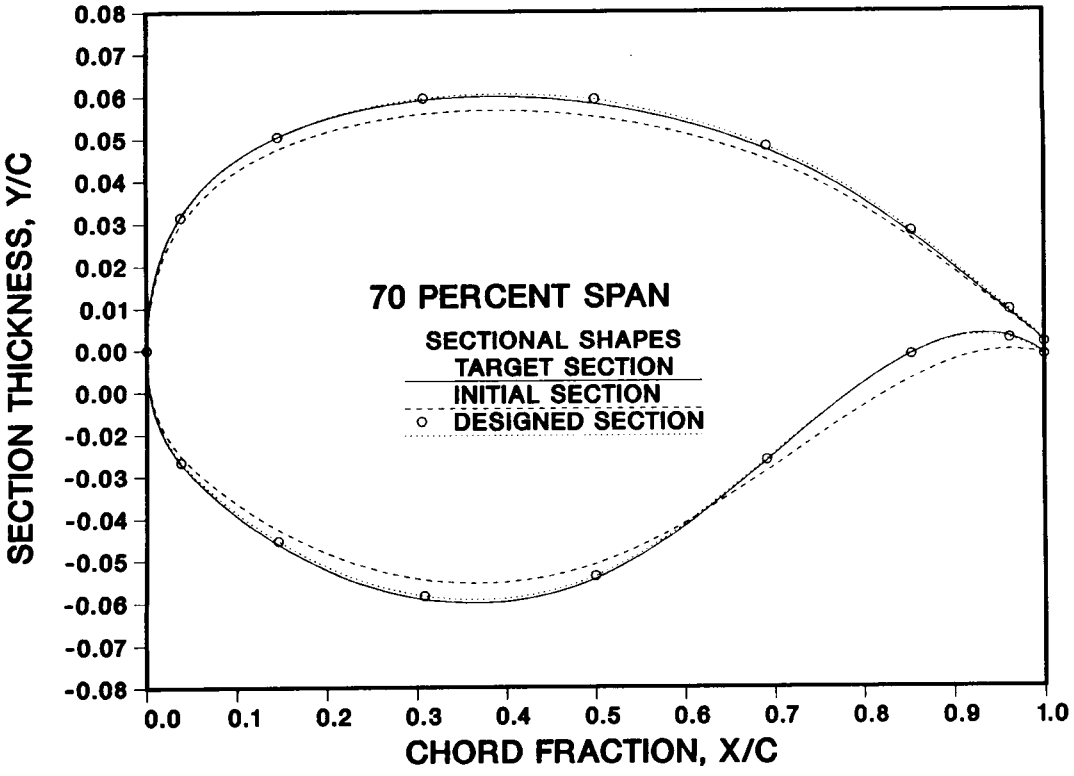

Figure 17. Comparison of section designed by TAW5D at 70 percent span for Lockheed Wing A wing body with target and first type of initial section.

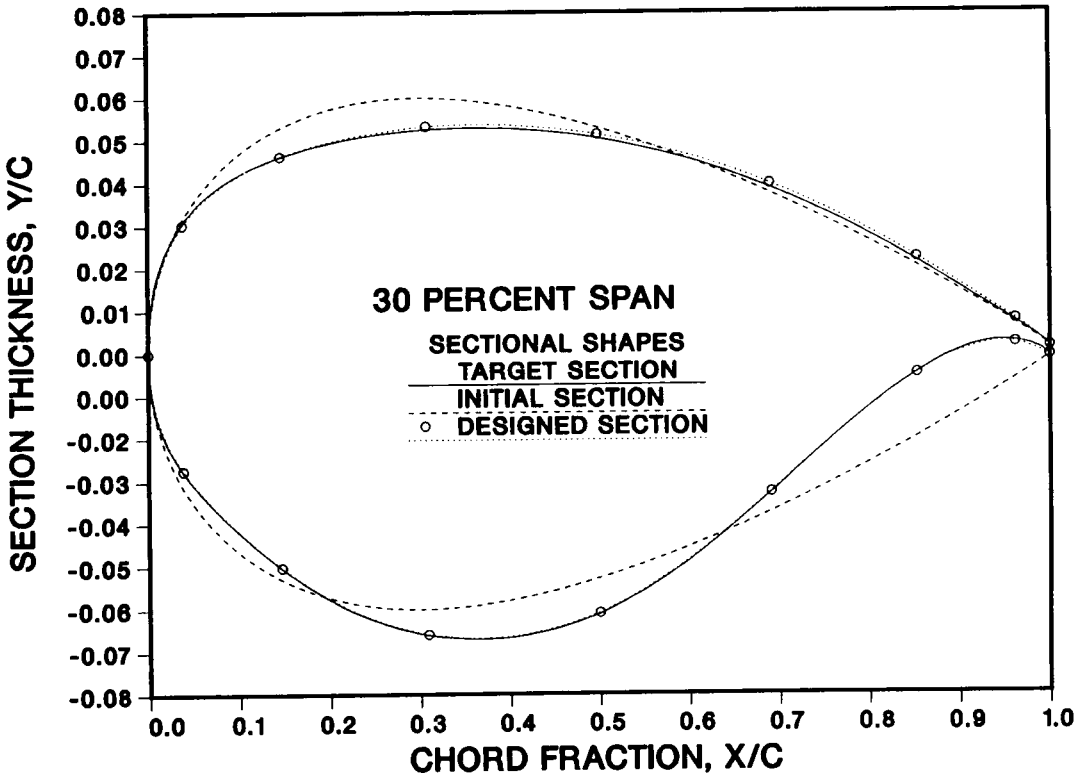

Figure 18. Comparison of section designed by TAW5D at 30 percent span for Lockheed Wing A wing body with target and second type of initial section.

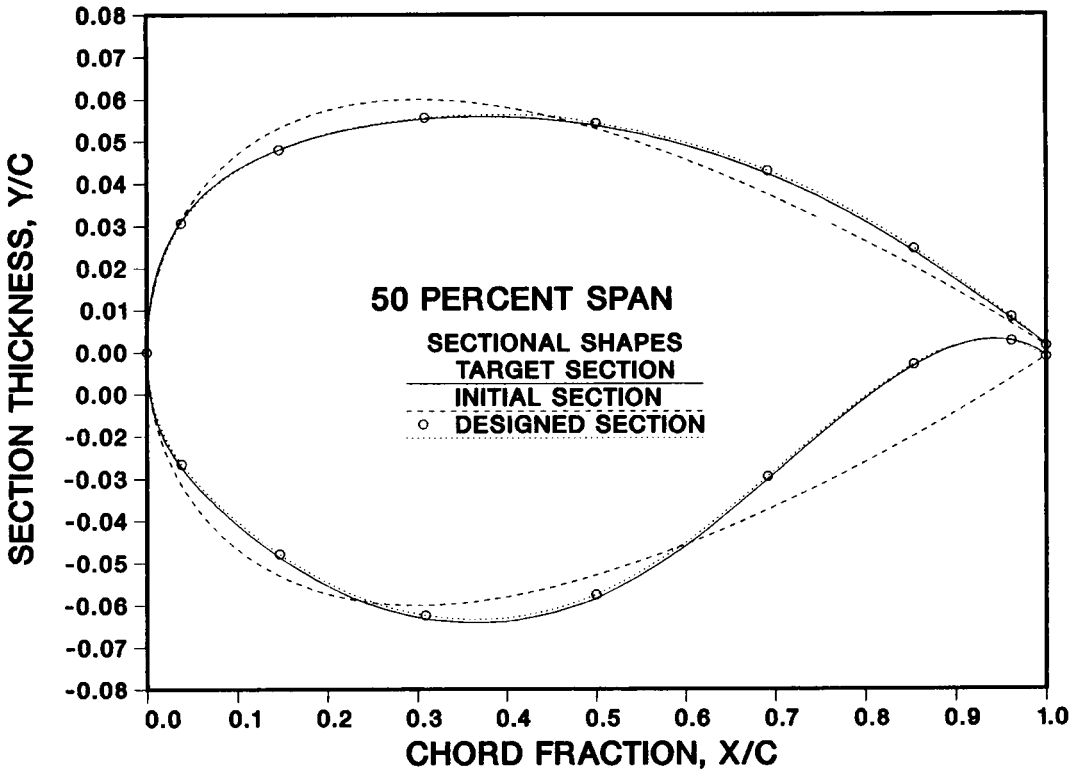

Figure 19. Comparison of section designed by TAW5D at 50 percent span for Lockheed Wing A wing body with target and second type of initial section.

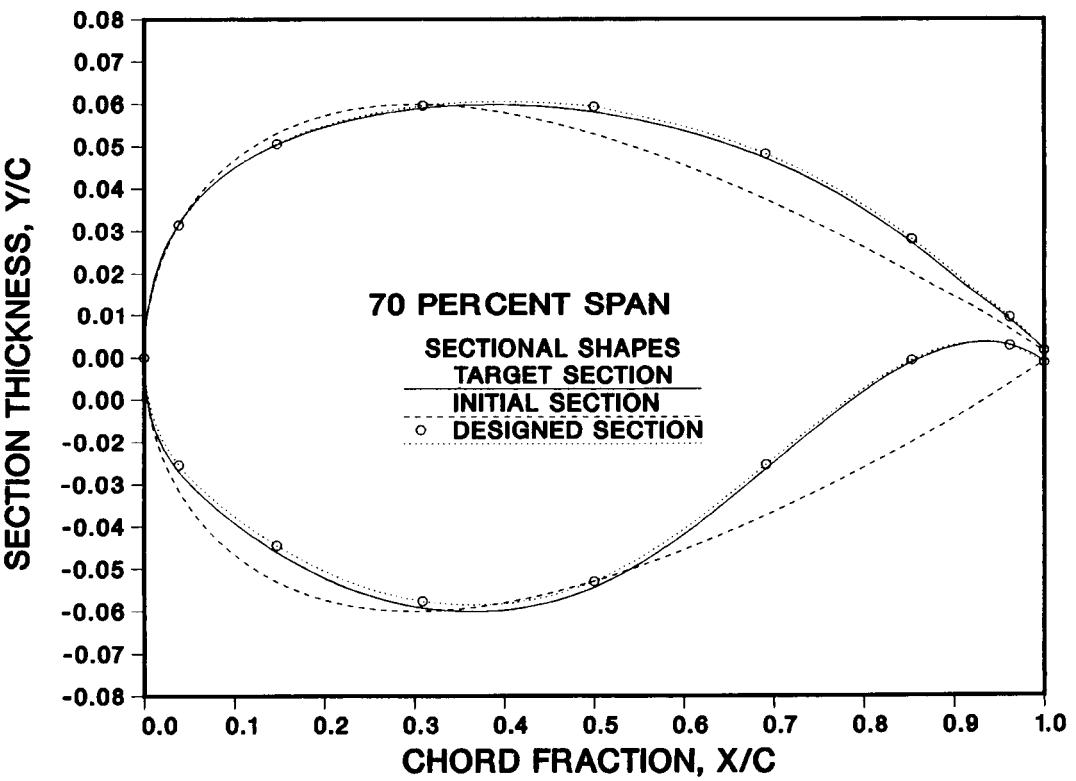

Figure 20. Comparison of section designed by TAW5D at 70 percent span for Lockheed Wing A wing body with target and second type of initial section.

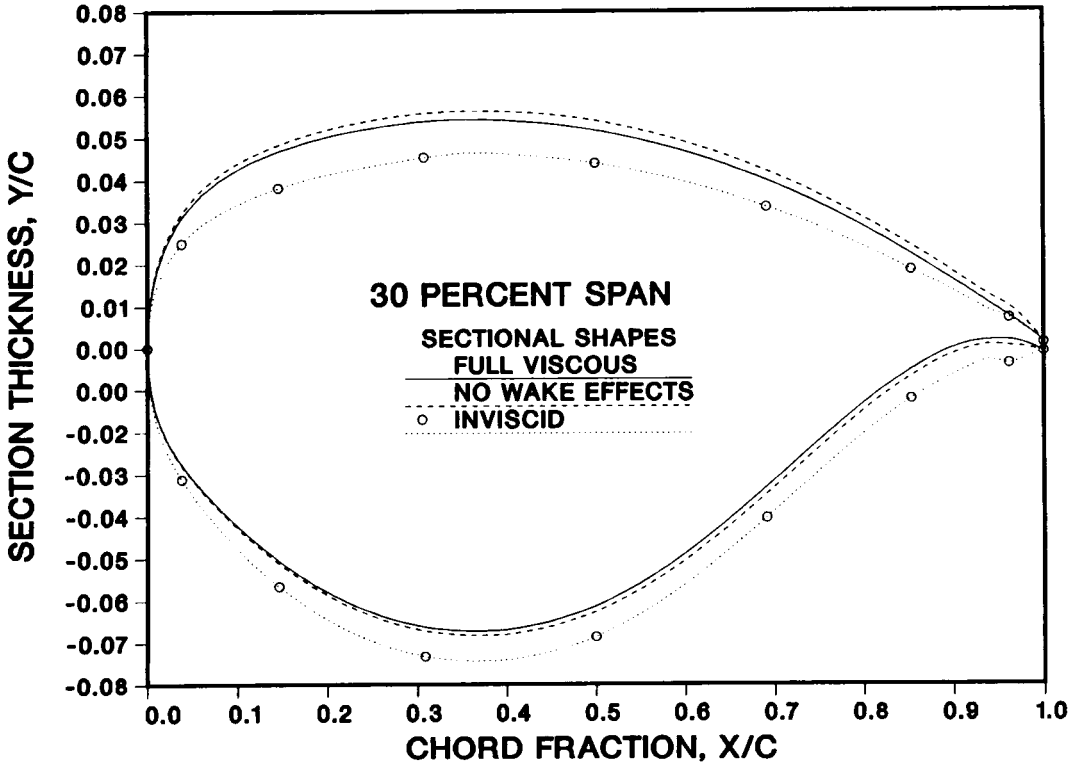

Figure 21. Comparison of sections designed at 30 percent span using different viscous interaction assumptions for Lockheed Wing 'A' wing body.

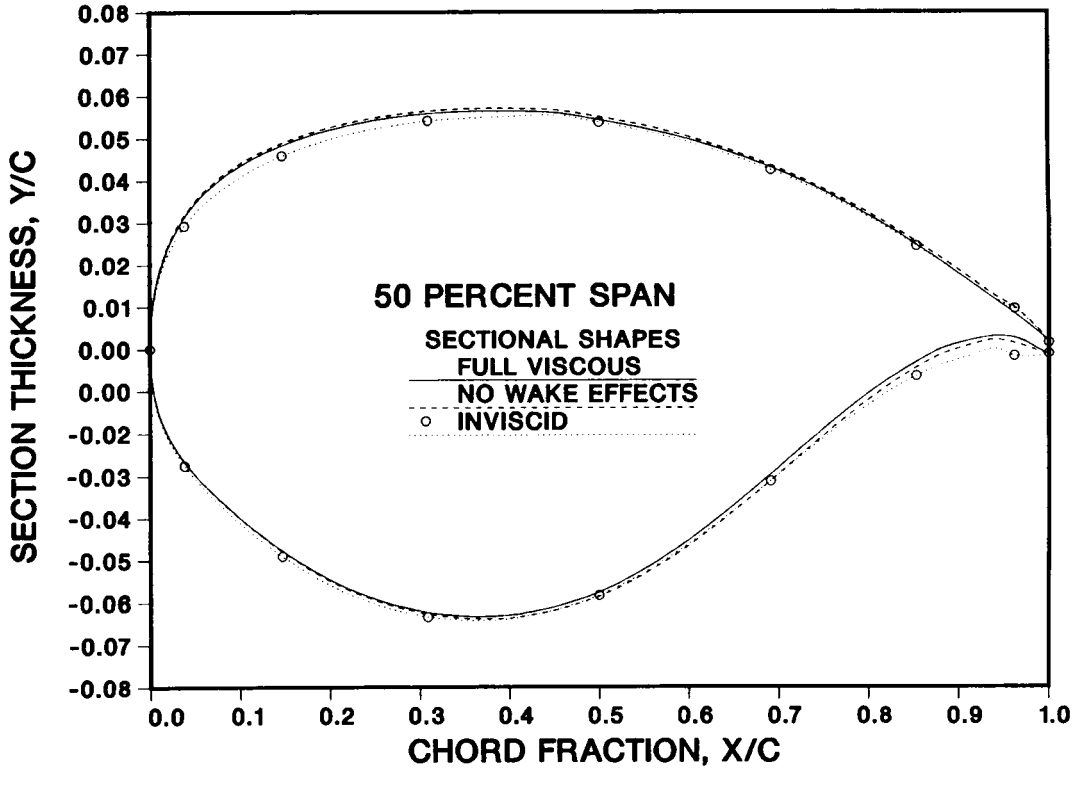

Figure 22. Comparison of sections designed at 50 percent span using different viscous interaction assumptions for Lockheed Wing 'A' wing body.

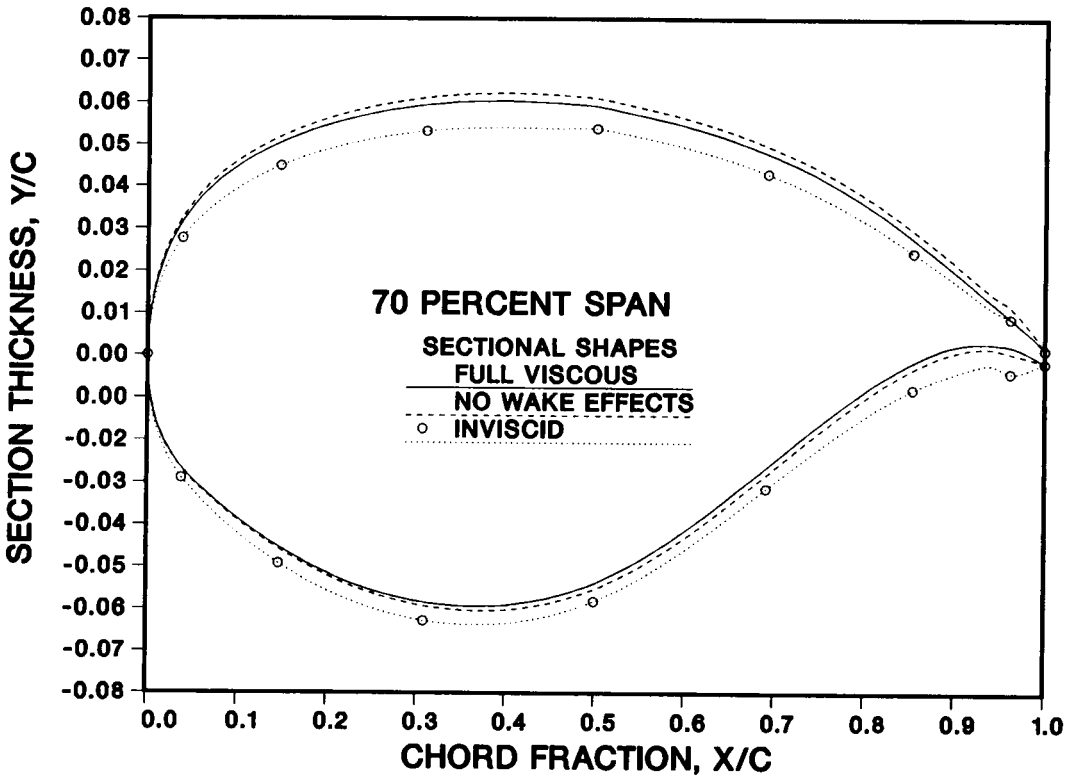

Figure 23. Comparison of sections designed at 70 percent span using different viscous interaction assumptions for Lockheed Wing 'A' wing body.

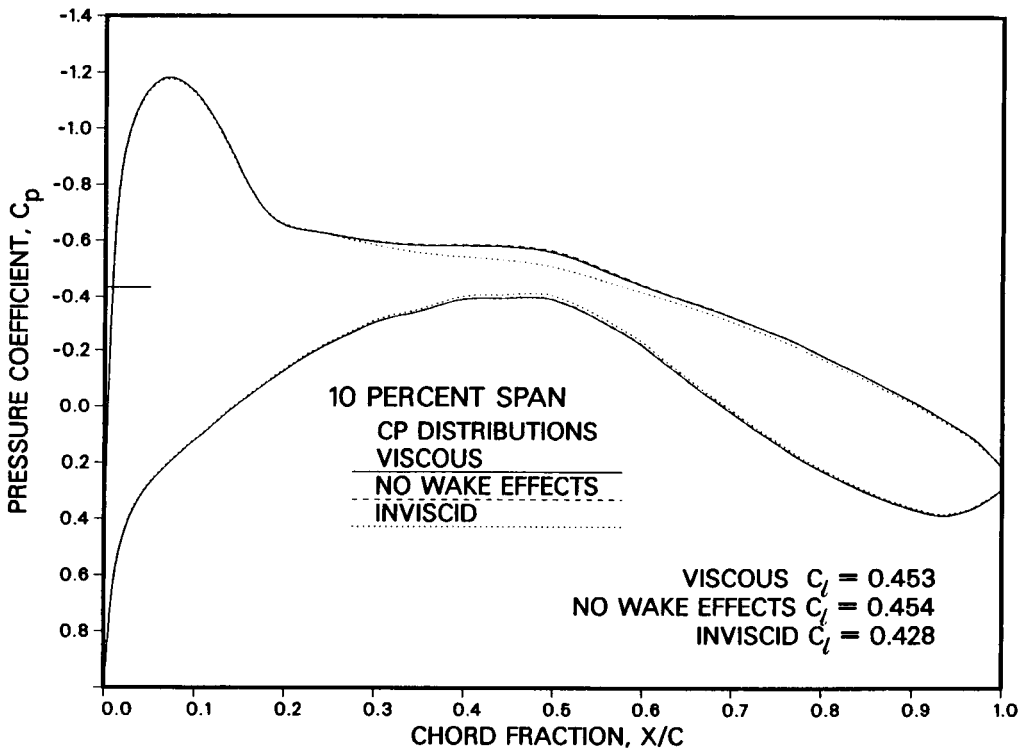

Figure 24. Comparison of pressures at 10 percent span obtained by viscous analyses of the wings designed using different viscous interaction assumptions (Lockheed Wing 'A', Mach = 0.8, AOA = 2 degrees, Reynolds No. = 24 million).

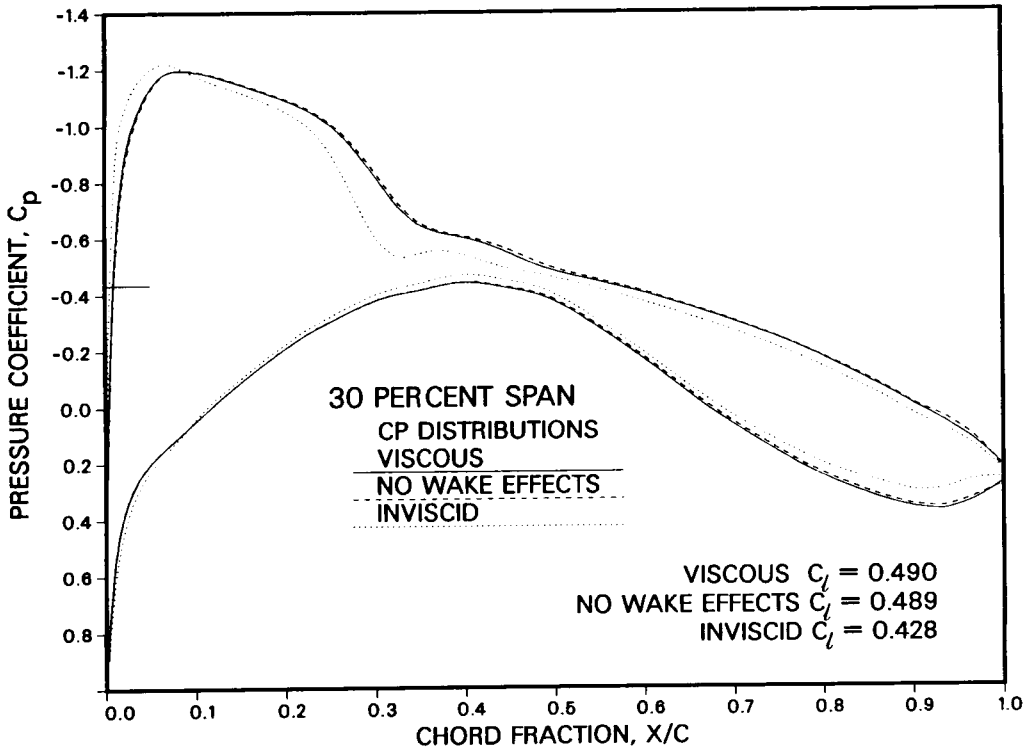

Figure 25. Comparison of pressures at 30 percent span obtained by viscous analyses of the wings designed using different viscous interaction assumptions (Lockheed Wing 'A', Mach = 0.8, AOA = 2 degrees, Reynolds No. = 24 million).

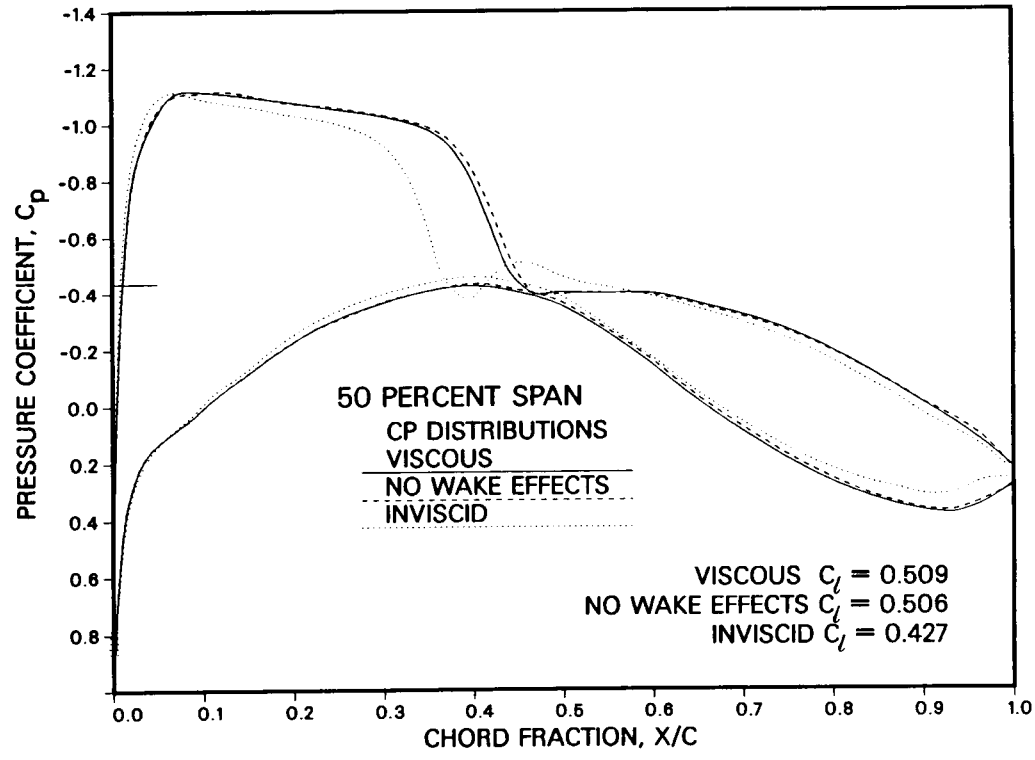

Figure 26. Comparison of pressures at 50 percent span obtained by viscous analyses of the wings designed using different viscous interaction assumptions (Lockheed Wing 'A', Mach = 0.8, AOA = 2 degrees, Reynolds No. = 24 million).

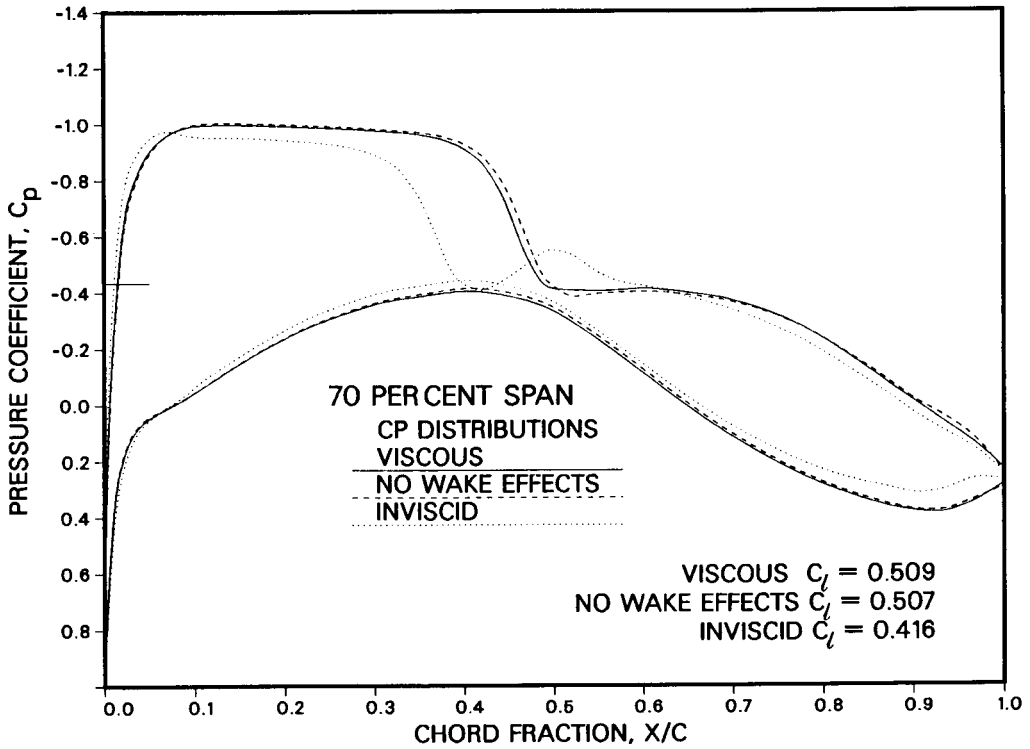

Figure 27. Comparison of pressures at 70 percent span obtained by viscous analyses of the wings designed using different viscous interaction assumptions (Lockheed Wing 'A', Mach = 0.8, AOA = 2 degrees, Reynolds No. = 24 million).

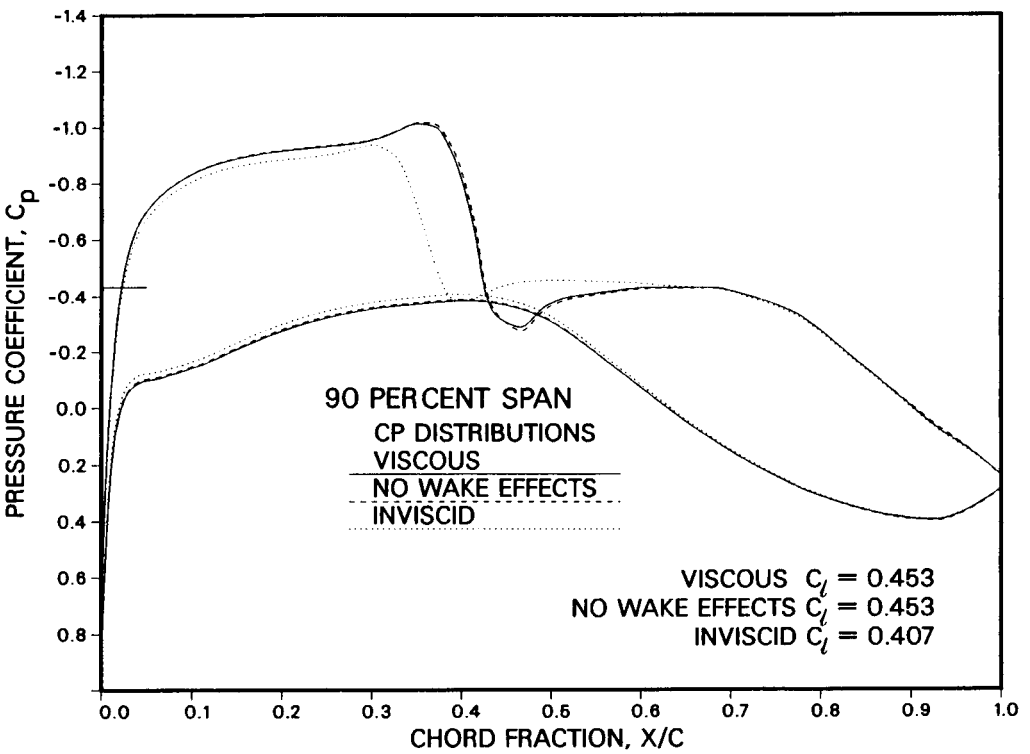

Figure 28. Comparison of pressures at 90 percent span obtained by viscous analyses of the wings designed using different viscous interaction assumptions (Lockheed Wing 'A', Mach = 0.8, AOA = 2 degrees, Reynolds No. = 24 million).